RESEARCH ARTICLE

Genetic mapping of distal femoral, stifle, and tibial radiographic morphology in dogs with cranial cruciate ligament disease

Eleni Healey[1☯], Rachel J. Murphy[1☯], Jessica J. Hayward[2], Marta Castelhano[3], Adam R. Boyko[2], Kei Hayashi[3], Ursula Krotscheck[3], Rory J. Todhunter[3]*

1 College of Veterinary Medicine, Cornell University, Ithaca, NY, United States of America, **2** Department of Biomedical Sciences and Cornell Veterinary Biobank, College of Veterinary Medicine, Cornell University, Ithaca, NY, United States of America, **3** Department of Clinical Sciences and Cornell Veterinary Biobank, College of Veterinary Medicine, Cornell University, Ithaca, NY, United States of America

☯ These authors contributed equally to this work.
* rjt2@cornell.edu

Abstract

Cranial cruciate ligament disease (CCLD) is a complex trait. Ten measurements were made on orthogonal distal pelvic limb radiographs of 161 pure and mixed breed dogs with, and 55 without, cranial cruciate partial or complete ligament rupture. Dogs with CCLD had significantly smaller infrapatellar fat pad width, higher average tibial plateau angle, and were heavier than control dogs. The first PC weightings captured the overall size of the dog's stifle and PC2 weightings reflected an increasing tibial plateau angle coupled with a smaller fat pad width. Of these dogs, 175 were genotyped, and 144,509 polymorphisms were used in a genome-wide association study with both a mixed linear and a multi-locus model. For both models, significant (p_{genome} <3.46×10^{-7} for the mixed and< 6.9x10^{-8} for the multilocus model) associations were found for PC1, tibial diaphyseal length and width, fat pad base length, and femoral and tibial condyle width at *LCORL*, a known body size-regulating locus. Other body size loci with significant associations were growth hormone 1 (*GH1*), which was associated with the length of the fat pad base and the width of the tibial diaphysis, and a region on CFAX near *IRS4* and *ACSL4* in the multilocus model. The tibial plateau angle was associated significantly with a locus on CFA10 in the linear mixed model with nearest candidate genes *BET1* and *MYH9* and on CFA08 near candidate genes *WDHD1* and *GCH1*. *MYH9* has a major role in osteoclastogenesis. Our study indicated that tibial plateau slope is associated with CCLD and a compressed infrapatellar fat pad, a surrogate for stifle osteoarthritis. Because of the association between tibial plateau slope and CCLD, and pending independent validation, these candidate genes for tibial plateau slope may be tested in breeds susceptible to CCLD before they develop disease or are bred.

Introduction

Cranial cruciate ligament disease (CCLD), one of the most common orthopedic disorders of dogs, results in partial to complete rupture of the cranial cruciate ligament (CCL), which in

turn, results in stifle destabilization, osteoarthritis, and hind limb lameness. Breeds at increased risk include the Newfoundland, rottweiler, Labrador retriever, bulldog, boxer, chow chow, American Staffordshire terrier, St. Bernard, West Highland white terrier, golden retriever, and Yorkshire terrier.[1, 2] In contrast, breeds with the least risk of developing CCLD include the miniature dachshund, dachshund, greyhound, Shih Tzu, miniature schnauzer, and Pekingese. [1] The cocker spaniel was reported in one study to have a reduced risk.[2] Within breeds, increased body weight has been associated with a higher risk of CCLD.[2] Several studies found that the incidence of CCLD increased with age, with the median age at diagnosis of 7–10 years.[3–5]

While studies have shown that spaying and neutering dogs can improve their health and increase their lifespan, these practices have been associated with an increased risk of developing CCLD in both male and female dogs.[1, 6] Some studies have reported a greater association between female dogs and CCLD than male dogs.[5, 7] However, others have noted no difference in disease incidence between the sexes.[6]

In addition to breed, body weight, age, and sex predispositions, there are differing conclusions regarding the role of the tibial plateau angle (TPA), or caudal tibial slope, in the pathogenesis of CCLD. Measurement of this angle is necessary for surgeries performed to correct CCLD in dogs, such as a tibial plateau leveling osteotomy (TPLO), which decreases TPA, and tibial tuberosity advancement, which is designed to neutralize this slope.

Several studies have found an association between increased TPA and CCLD, encouraging the use of TPA as a measurement for CCL strain and to predict CCLD.[8, 9] Other studies have found no association between increased TPA and CCLD, and, as a result, have cautioned against the use of TPA to determine the risk of CCLD.[10] Furthermore, while one study did not conclude TPA to be significantly different between dogs with CCLD and dogs without CCLD, the findings suggested that increased TPA may be associated with increased severity of stifle radiographic osteoarthritis (OA) in dogs with CCLD.[11] In addition, another study found a separate yet related measurement, the anatomical-mechanical axis angle, to more accurately predict CCLD than TPA.[12]

Cranial cruciate ligament disease is a complex trait controlled by genetic factors with environmental regulation. In linkage analysis of 271 Newfoundland dogs, quantitative trait loci (QTL) for CCLD were found on canine chromosome (CFA) 03, 05, 13, and 24[13] and a genome wide association study (GWAS) pointed to loci on CFA 01, 03 and 33 with CCLD in the same pedigree.[14] Single nucleotide polymorphisms (SNPs) were located within genes involved in neurological regulation suggesting the potential effect of neural dysfunction on CCLD onset and progression.[14] Another study employed candidate gene analysis in Newfoundlands, Labrador retrievers, Staffordshire bull terriers, and rottweilers to genotype 196 SNPs across 28 candidate genes, which were selected based on their potential contribution to the structure of the CCL or CCLD progression.[15] No polymorphisms in candidate genes encoding collagen and other components of the extracellular matrix were discovered.[15]

Most recently, a GWAS for CCLD, including 237 Labrador retrievers, reported one SNP within a 5kb haplotype block on CFA24 which met genome-wide significance.[16] Within this block, 9 genes influenced tissue homeostasis and, thus, might impact CCL function.[16] Our most recent GWAS of 670 dogs of different breeds found three SNPs associated with CCLD; one each on chromosomes 7, 8, and 9, with *CLMN* and *DYN* as positional candidate genes. [17] Most recently, Baker[18] reported a multivariate GWAS based model of CCLD, TPA, and tibial tuberosity width in which they identified 3 loci with moderate evidence of association that were not previously associated with CCLD. A locus on CFA01 was associated with both CCLD and tibial tuberosity width located within *ROR2*, a gene implicated in cartilage and bone development. A polymorphism on CFA04 was associated with both CCLD and TPA and

was within *DOCK2*, a gene shown to promote immune cell migration and invasion in synovitis, an important predictor of CCLD. A third locus on CFA23 was associated with only CCLD and was near a long non-coding RNA (lncRNA).

Principal component analysis (PCA) reduces many measurements into their correlated components with each PC independent of the others and these PCs can be analyzed like a traditional phenotype. We have used PCA to analyze the genetic basis of other canine orthopedic traits including pelvic morphology.[19] The present study used PCs of 10 pelvic limb radiographic measurements, as well as the individual measurements (some of which are correlated to CCLD and secondary OA), in a linear mixed and a multi-locus model GWAS. We report significant associations of the TPA with loci on chromosomes 8 and 10. In addition, a locus on chromosome 3 (*LCORL*), previously associated with body size in several species, was significantly associated with PC1 and individual pelvic limb measurements. Mutations in candidate genes in these associated genomic regions may provide further insight into the genetic predisposition to CCLD and its environmental regulation. Veterinarians, owners and dog breeders need better tools to inform preventative strategies and breeding decisions, and better therapy to prevent CCLD and the secondary OA that encumbers affected dogs.

Materials and methods

Dogs

We measured a subset of stifle radiographs which were used to diagnose stifle OA resulting from CCLD in a previous GWAS[17, 20] and radiographs on additional dogs were added for the PCA. Dogs had stifle radiography at the Cornell University Hospital for Animals and a subset of these dogs had been genotyped. The full set included 161 control dogs and 55 dogs with CCLD. Dogs included in this study represented 38 pure breeds and mixed-breed dogs.

Radiographic measurements

Some dogs had lateral stifle radiographs taken with the long axes of the femur and stifle at 90° (as is customary for preparation for TPLO surgery), others had lateral radiographs taken with the femur and tibia at ~135° (as is customary for tibial tuberosity advancement surgery), while some radiographs were taken with the femur and tibia at angles in between 90°and 135°.

Both lateral and cranial-caudal radiographic projections of one or both distal pelvic limbs including the stifle, the tarsus and the distal femur were required for inclusion of the dog in this study. If any abnormalities altering bony dimensions or alignment of the femur or tibia were noted, including extensive stifle bony proliferation/osteolysis or healed and malaligned fractures, the dog was excluded. Dogs less than three years of age were excluded due to their low number. If multiple studies were available, the most recent study was selected for analysis, unless the dog was better positioned on earlier radiographs. Radiograph positioning criteria for lateral projections were based on the superposition of the femoral condyles. Positioning criteria for cranial-caudal projections were evaluated on condyle and proximal tibial symmetry and patellar location in the center of the trochlea groove. The best positioned single limb radiograph was used from each dog.

Radiographs were measured in PACS imaging software (https://www.carestream.com/en/us/pacs-software). Each radiograph was scaled to the original size of the patient using a 100 mm internal calibration tool placed at bone level when the image was taken. Ten measurements were generated for each patient; six measurements on the lateral projection and four on the cranial-caudal projection (Table 1; Fig 1).

The same person (EH) made all the measurements after instruction from an experienced surgeon (RJT). We tested the TPAs for internal consistency by randomly sampling 20 individual radiographs and remeasuring the TPA, resulting in a correlation of 0.86.

A Shapiro-Wilk test was used to assess if the measurements were normally distributed. All measurements, except the TPA, were not normally distributed ($p < 0.05$). All the measurements, except the TPA, were significantly different in males compared to females based on an unpaired 2-tailed t-test. To adjust each measurement according to the dog's sex, each measurement was modeled as a linear function of sex. The Box-Cox command in the R package "MASS" was used to transform the measurements (Figure A in S1 File). Unpaired 2-tailed t tests were used to compare body weights, age, TPA, and transformed fat pad height and width between the dogs with and without CCLD. $P < 0.05$ was considered significant.

Principal component analysis (PCA)

Principal component analysis was performed on 10 sex-adjusted and transformed radiographic measurements of 216 stifles using the prcomp function in R [21] Body weights, expressed as body weight$^{0.303}$ based on a Box-Cox transformation to normalize the distribution of body weight across breeds, were available for 151 dogs with CCLD and 55 control dogs. We regressed PC1 against body weight to determine if there was a significant relationship between them with $P < 0.05$ considered significant.

Genome-wide association study (GWAS)

DNA was stored at the Cornell Veterinary Biobank (https://www.vet.cornell.edu/departments/centers/cornell-veterinary-biobank). Genotypes were used from previous reports.[17, 20] In brief, genotyping was performed on a semi-custom Illumina 173k CanineHD mapping array,

Table 1. Radiographic measurements of the stifle and tibia used to derive principal components and phenotypes for genome wide association study.

Lateral projection	Radiographic measurement
Tibial plateau angle	One line connecting the center of the talus to the center of the tibial intercondylar eminences. A second line along the tibial condyles connecting the point just caudal the insertion of the cranial cruciate ligament and extending caudally to pass through the caudal tibial plateau as it deviated distally to join the proximal tibial metaphysis. The obtuse angle between these two intersecting lines was the TPA.
Tibia length	A line originating at the center-point of the lateral malleolus of the fibula and ending at the proximal intercondylar eminence.
Tibial diaphyseal width	The distance between the outside cortices at the mid tibial diaphysis
Tibial tuberosity length	A line connecting the proximal and distal tibial tuberosity
Infrapatellar fat pad height	The distance at the caudal edge of the patellar ligament from the distal patella to its insertion on the tibial tuberosity
Infrapatellar fat pad width	At its widest point, a line perpendicular to the height of the infrapatellar fat pad caudal to the edge of the soft tissue opacity within the joint space
Cranial Caudal Projection	
Tibial diaphyseal width	At the mid-point of the tibial diaphysis, the width to each outer cortex
Femoral condyle width	A line perpendicular to the long axis of the femur at the level of the base of the intercondylar fossa, extending from the medial to the lateral femoral condyles
Femoral notch width	A line perpendicular to the long axis of the femur at the mid-point of the intercondylar fossa and extending between the axial borders of the femoral condyles
Tibial plateau width	A line perpendicular to the long axis of the tibia at the proximal aspect of the tibial metaphysis
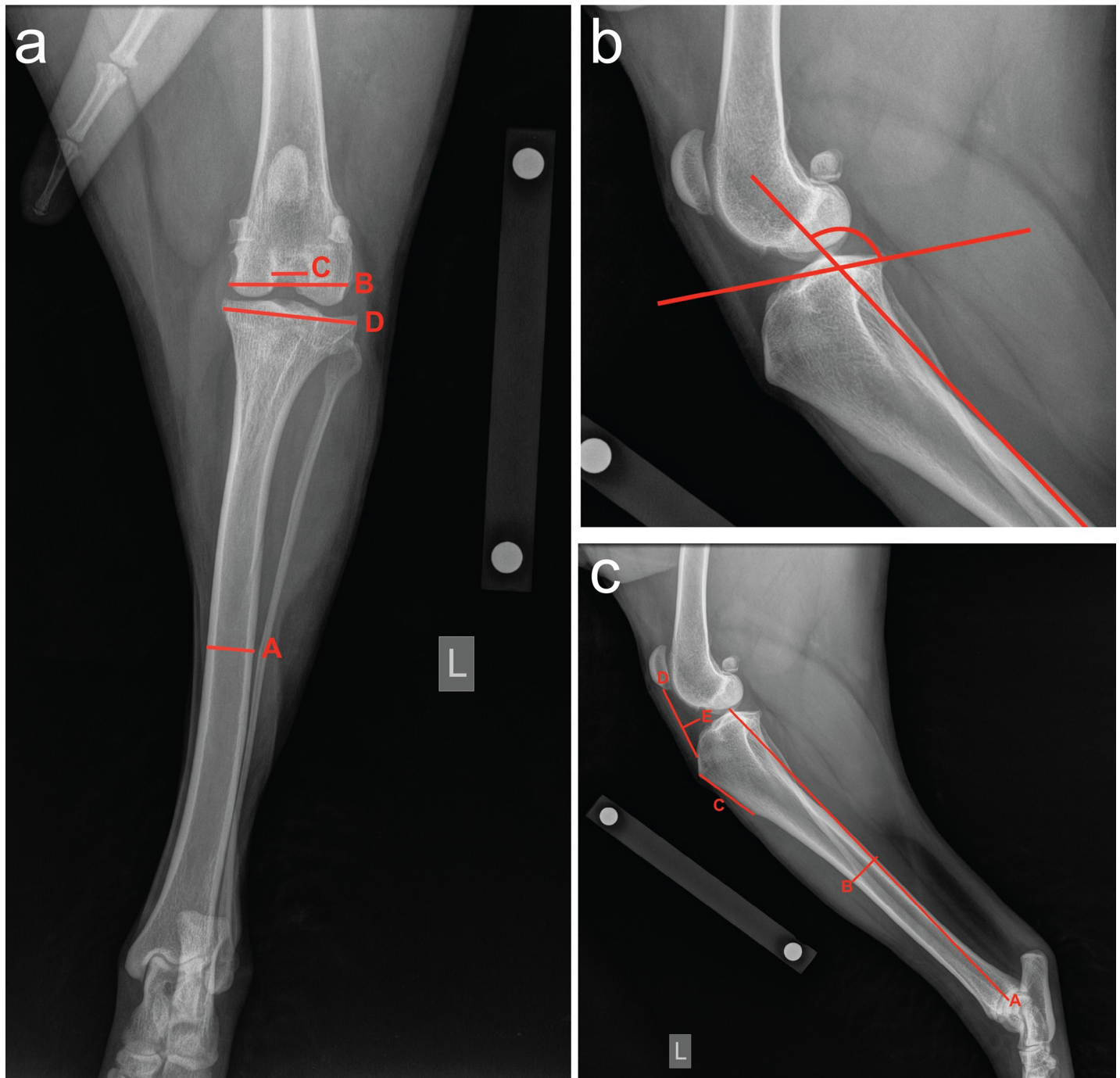
Fig 1. Illustration of radiographic measurements of dog stifles and tibiae. Panel A. Cranial-caudal radiograph shows the mid-diaphyseal tibial width (A), the femoral condyle width (B), the femoral notch width (C), and the proximal tibial width (D). Panel B. Lateral radiograph of proximal tibia illustrating the tibial plateau angle (see Table 1 for description). Panel C. Lateral tibial radiograph illustrating the tibial length (A), the tibial diaphyseal width (B), the tibial tuberosity length (C), the infrapatellar fat pad height (D), and the infrapatellar fat pad width (E).

https://doi.org/10.1371/journal.pone.0223094.g001

supplemented with 12,143 markers for a total of 185,805 markers [see PLINK genotype files by Hayward[20] that are deposited in Dryad (datadryad.org, doi:10.5061/dryad.266k4)]. PLINKv1.07[22] was used to remove SNPs with a genotyping rate below 95%, discordant

SNPs between duplicate samples, SNPs that deviated from Hardy-Weinberg equilibrium, and any mitochondrial or Y chromosome SNPs with heterozygous calls [20]. After these filtering steps, 180,117 SNPs remained for analyses. For GWAS, the PCs and the transformed measurements were analyzed in a linear mixed model using the program GEMMA v.0.94[23] which included a relatedness matrix (estimated using centered genotypes) and the Wald Test was used to determine P-values. In the model $Y = W\alpha + X\beta + u + \varepsilon$, where W is a $n \times (c+1)$ matrix of covariates, α is the $(c+1)\times 1$ vector of covariate effects including intercept, X is the genotype data, β is the effect size, u is a random effect (including the $n\times n$ relatedness matrix), ε is a random error term, the fixed effects are W, α, β and the random effects (u and ε), are assumed to have a normal distribution. We excluded SNPs with a minor allele frequency (MAF) <5%, resulting in 144,509 SNPs remaining for the GWAS, and a significance threshold of $P < 3.46 \times 10^{-7}$ (the Bonferroni-adjusted genome wide P-value<0.05) was used.

In addition to the linear mixed model, we implemented a multi-locus model using the R package FarmCPU[24], which reduces false negatives which can be observed in linear mixed model GWAS. We used the default parameters (MAF threshold of 5%, maximum of 10 loops or iterations, Bonferroni-corrected threshold calculated with alpha = 0.01 producing p_{genome} $< 6.9 \times 10^{-8}$) and included a population structure matrix as a covariate file. This covariate file consisted of the first 10 PCs from a PCA of the genotypes on all 175 dogs. Manhattan and Quantile-Quantile (QQ) plots were created in R[21]. QQ plots were used to show the distributions of our observed GWAS *P*-values compared to the expected *P*-values. Significant associations of markers and CCLD deviate from a uniform distribution, that is, they do not follow the diagonal X = Y line on a QQ plot.

Results

Dogs

The 161 dogs with CCLD and 55 dogs without CCLD included 77 Labrador retrievers, 20 golden retrievers, 18 mixed breed dogs, 17 German shepherd dogs, 16 rottweilers, and 62 other pure breed dogs with less than 10 dogs per breed. Of these, 175 dogs were genotyped. Descriptive statistics for the 10 radiographic measurements (Table A in S1 File) are shown in Table 2.

Body weight for CCLD dogs (39.1±SD = 11.0 kg) was significantly higher than control dogs (28.1±15.2 kg) (unpaired t-test, t = 5.508, df = 202, P<0.0001). Dogs with CCLD were significantly younger (65±32 months) than control dogs (84±51 months) (unpaired t-test, t = 3.392, df = 201, P = 0.0008). Even though the difference was not large, the TPA was significantly higher in dogs with CCLD (116.6±3.9˚) than in control (114.5±4.8˚) dogs (unpaired t-test, t = 3.261, df = 214, P = 0.0013). Fat pad width was significantly larger (2.5±0.3 mm) in CCLD dogs than in control (2.3±0.6 mm) dogs (unpaired t-test, t = 3.163, df = 214, P = 0.0018) and

Table 2. Descriptive statistics summary of the 10 radiographic measurements described in Table 1. All measurements except the tibial plateau angle are in mm. The number in parentheses after the column heading is the number used for the Box-cox transformation as described in the Materials and Methods Section.

	Tibial plateau angle	Tibia length (1.9)	Lateral diaphysis (2.0)	Tuberosity length (1.0)	Fatpad base (0.7)	Fatpad height (0.1)	Cranial diaphysis (1.9)	Femoral condyle (1.7)	Femoral notch (1.8)	Tibia condyle (2.0)
Min.	01.0	32.6	0.2	0.9	0.9	0.9	0.3	1.1	0.2	2.6
LQ	13.7	281.7	2.3	2.1	2.3	0.1	2.2	7.8	1.0	15.8
Median	116.2	329.7	2.6	3.3	2.5	0.1	2.8	9.3	1.2	19.3
Mean	116.1	329.2	2.7	3.3	2.4	0.1	2.7	9.3	1.2	19.2
UQ	118.9	387.4	3.1	3.7	2.7	1.0	3.1	10.5	1.4	23.1
Max.	126.2	829.3	5.4	7.4	3.5	1.1	6.1	17.8	2.6	39.3

fat pad height was significantly smaller (0.98±0.02 mm) in CCLD dogs than in control (1.0 ±0.03 mm) dogs (unpaired t-test, t = 6.795, df = 214, P = 0.0001).

Principal component analysis

Body weight and PC1 were significantly correlated (r = 0.79, t = 15.896, df = 164, P<0.001)). The first four PCs explained almost 94% of the total variance (Table 3).

A plot of PC1 against PC2 showed that the dogs with CCLD tended to cluster closer together more than the control group (Fig 2) but not according to sex of the dogs (Fig 3). Each measurement was weighted approximately equally for PC1 except for the TPA and the fat pad height (Table 4).

The main contributions to PC2 came from the TPA and the fat pad height but in the opposite direction. That is, as the TPA increased the fat pad height decreased as expected because as the TPA increased the dogs were more likely to have CCLD, and hence fat pad compression from synovitis and OA. However, not every dog followed this association because the main weightings on PC3 were from the same two measurements but in this case, lower angles and smaller fat pad height were seen. For PC6, longer tibial tuberosities and wider femoral and tibial condyles were weighted positively while the fat pad base was negatively weighted and it provided the major contribution to PC6.

Genome wide association study

In the 175-dog subset with both genotypes and radiographs, a well-recognized locus CFA03:91114590 which contains *LCORL*, a gene which contributes strongly to body size of many species, including the dog,[4, 20, 25, 26] was significantly associated with PC1 (Fig 4), in both the linear mixed model and the multi-locus model.

This locus was also associated significantly with tibial length (Figure B in S1 File), lateral tibial diaphyseal width (Figure C in S1 File), tibial tuberosity length (Figure D in S1 File), fat pad base (Figure E in S1 File), and femoral (Figure F in S1 File) and tibial (Figure G in S1 File) condyle width in both the linear mixed model and the multi-locus model (Tables 5 and 6).

Another previously observed canine body size locus[27–29], at CFA39:82,673,593 bp near the genes *IRS4* and *ACSL4*, was significantly associated with femoral and tibia condyle width in the multi-locus model only. A locus at CFA23:11,346,684 with the closest candidate genes, *TRAK1* and *CCK*, was associated significantly with tibial tuberosity length in both models, and also with PC6 in the linear mixed model.

Table 3. Eigenvalue, variance, and cumulative variance of the 10 principle components.

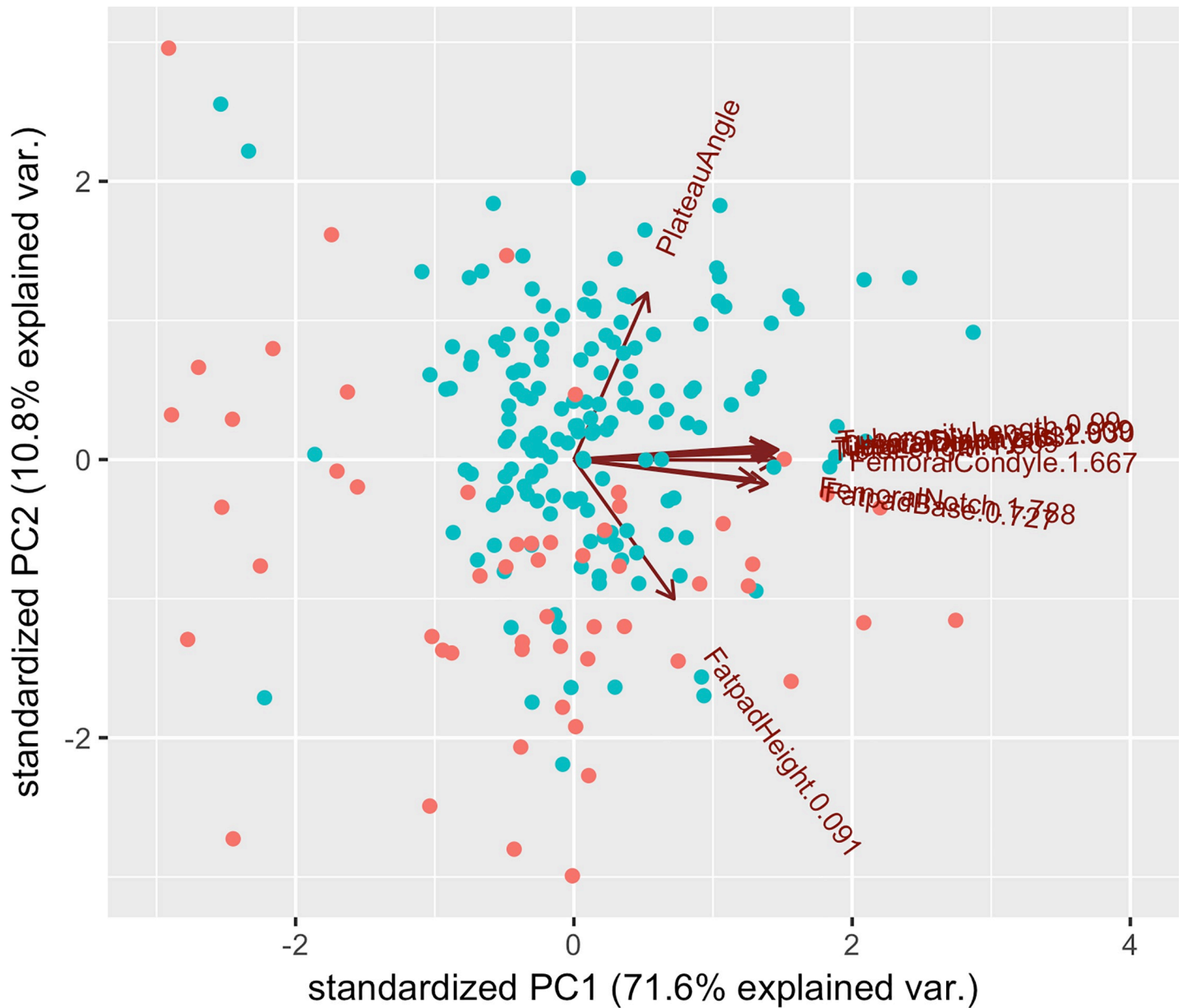|	Eigenvalue	Variance	Cumulative Variance
PC1	7.3	73.0	73.0
PC2	1.1	10.8	83.8
PC3	0.8	6.8	90.6
PC4	0.3	3.1	93.7
PC5	0.2	2.1	95.8
PC6	0.1	1.1	97.3
PC7	0.1	0.1	98.2
PC8	0.1	0.9	99.1
PC9	0.1	0.6	99.8
PC10	0.0	0.2	100.0

Fig 2. Plot of PC1 and PC2 values according to whether a dog had CCLD (red) or was a control (blue).

In general, we saw many more significant associations using the multi-locus model than the linear mixed model (Figures H-R in S1 File), but there were several significant associations that were only seen in the linear mixed model, as follows. PC6 was significantly associated with locus CFA35:1,776,352 with the closest candidate gene *FOXQ1* (Fig 5).

Tibial plateau angle was significantly associated with a locus on CFA10:28,002,796 with nearest candidate genes *BET1* and *TXN2* about 50kb upstream and *MYH9* (Fig 6) about 80 kb downstream.

The locus CFA08:30,830,592 near candidate gene *WDHD1*, was also associated significantly with TPA. Growth hormone 1 (*GH1*) on CFA09:12074972, which regulates body mass, was associated significantly with the length of the fat pad base and the size of the tibial diaphysis.
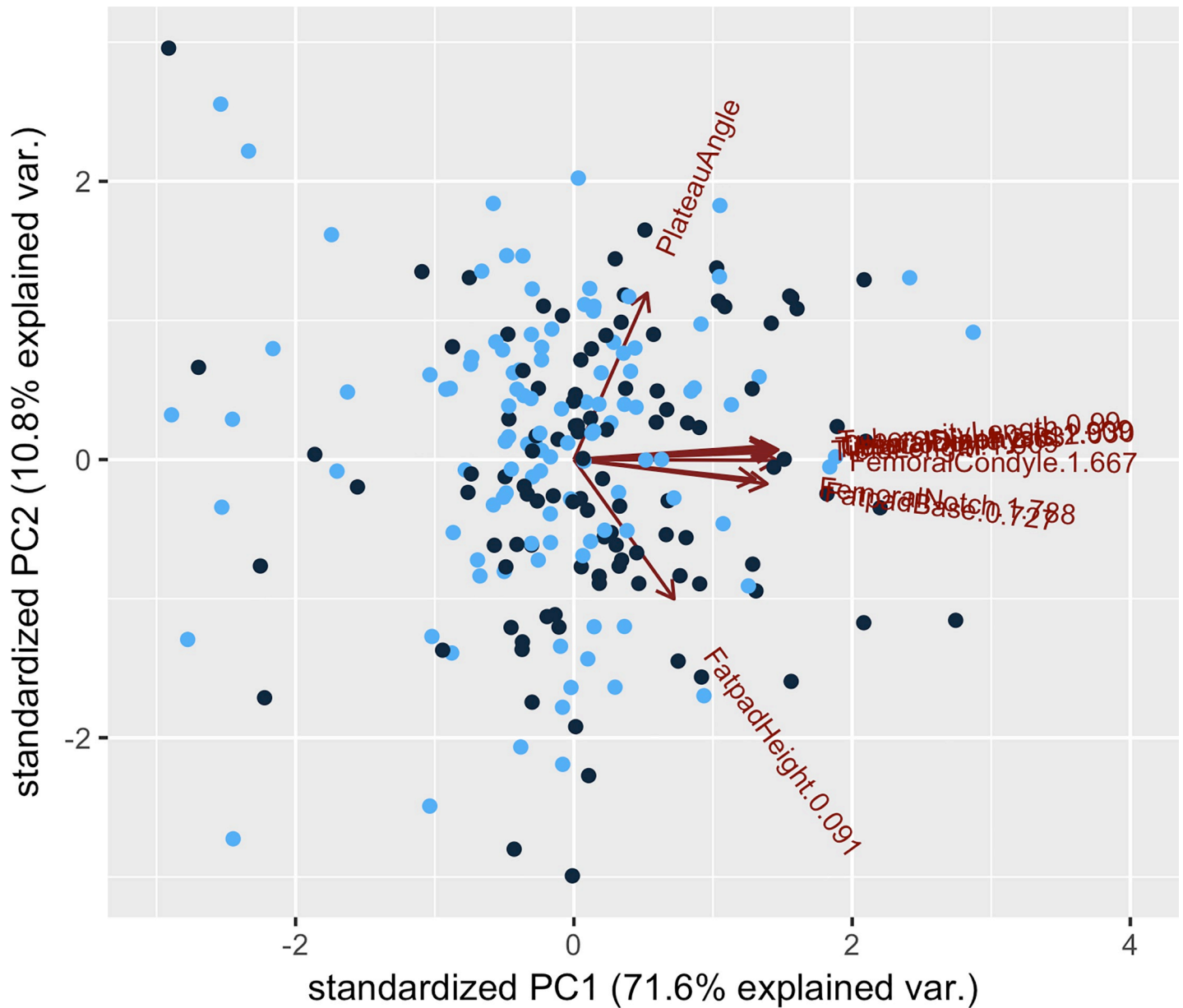
Fig 3. Plot of PC1 against PC2 values for male (black) and female (blue) dogs.

Using the multi-locus model, we also saw significant associations on CFA6:74,641,230 with PC1 and the cranial diaphyseal length (Fig 7), on CFA5:29,898,790 with tibial tuberosity length, and on CFA5:12,118,506 with femoral and tibia condyle width (Table 6). All these significant associations are shown in the respective QQ plots as a tail that deviates well above the diagonal X = Y line.

Discussion

Rupture of the cranial cruciate ligament remains a universal major disorder for mixed and pure breed dogs. In 2005, it was estimated that owners spent $1.32 billion for the treatment of CCLD in the United States,[30]. In 97 primary practices surveyed in England in 2015, ~ 0.5–

Table 4. Composition of the 10 principal components (PCs) with the weighting of each individual pelvic limb measurement.

Measurement Location	PC 1	PC 2	PC 3	PC 4	PC 5	PC 6	PC 7	PC 8	PC 9	PC 10
Plateau angle	0.13	0.75	-0.63	-0.04	0.07	-0.05	0.03	-0.01	0.00	-0.00
Tibial length 1.91	0.35	0.03	0.02	0.22	-0.40	0.16	-0.19	-0.12	-0.76	-0.07
Lateral diaphysis 2.03	0.35	0.05	0.11	0.12	0.32	0.04	-0.83	-0.03	0.25	0.02
Tuberosity length 0.99	0.34	0.06	0.04	0.41	-0.44	0.35	0.19	0.37	0.48	-0.01
Fat pad base 0.73	0.34	-0.11	-0.01	0.27	-0.14	-0.84	0.12	-0.19	0.13	-0.04
Fat pad height 0.09	0.18	-0.63	-0.71	0.07	0.16	0.16	0.02	-0.00	-0.01	0.06
Cranial diaphysis 1.91	0.34	0.05	0.20	0.12	0.61	-0.05	0.32	0.51	-0.29	0.01
Femoral condyle 1.67	0.36	-0.00	0.11	-0.24	0.15	0.23	0.24	-0.44	0.14	-0.68
Femoral notch 1.79	0.32	-0.09	-0.03	-0.77	-0.29	-0.17	-0.12	0.41	0.00	0.00
Tibia condyle 2.03	0.36	0.04	0.15	-0.19	0.06	0.17	0.24	-0.44	0.14	0.68

https://doi.org/10.1371/journal.pone.0223094.t004

0.6% of 171,000 dogs suffered from CCLD.[2] Extending this proportion to the approximately 70 million dogs in households in the USA, about 400,000 US dogs might be diagnosed with CCLD annually. In England, about 20% of the affected dogs, especially the heavier, insured dogs, were referred to surgeons for corrective osteotomy procedures. The preference for osteotomy procedures aligns with the preference of USA surgeons.[31] If the approximate total cost of an osteotomy procedure is currently $4,000 in the USA, a likely underestimate, over $3 billion might be spent per year, currently, for surgical correction of CCLD by the American dog-owning public to treat CCLD. This cost ignores the cost of extracapsular and intra-articular repairs, the long-term disability caused by the secondary osteoarthritis, the cost of complications due to the surgical procedures, medical management, and the additional costs for dogs with bilateral CCLD. Therefore, finding a solution to this debilitating trait and its secondary OA is a worthy endeavor.

Because CCLD is a complex trait with heritability in Newfoundland dogs[32] estimated at 0.27, an estimate similar to that of canine hip dysplasia, one approach to reduce the prevalence of the disease is by breeding dogs of improved genetic quality. Unfortunately, CCLD is a late onset disease compared to the earlier age-of-onset of canine hip and elbow dysplasia. Therefore, efforts to reduce the prevalence of the trait require the discovery of other features of the
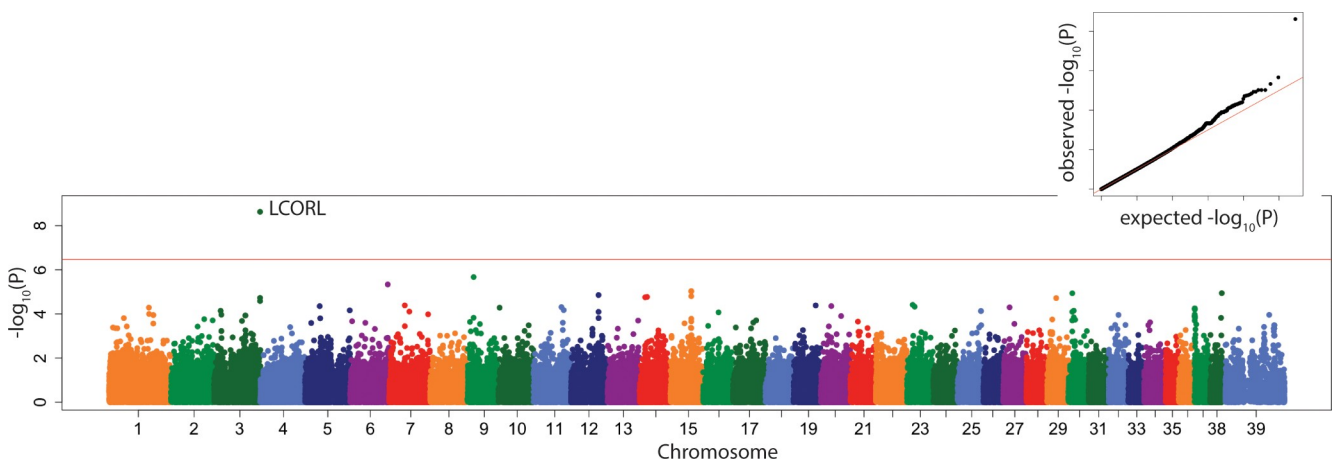

Fig 4. Manhattan plot of linear mixed model GWAS of PC1. Marker position plotted on the X axis against $-\log_{10}(P)$ on the Y axis. The Bonferroni adjusted genome wide p value threshold is drawn as the red line across the plot. QQ plot of expected $-\log_{10}(P)$ for no association against observed $-\log_{10}(P)$ is shown as insert.

https://doi.org/10.1371/journal.pone.0223094.g004

Table 5. Genome wide significant marker associations of 10 radiographic morphologic measurements and their principal components, chromosome position, effect size, p value and candidate gene(s) in the associated interval following a linear mixed model GWAS performed in GEMMA.

Phenotype	Chr	Position (bp)	Effect size	P-value	Candidate Genes
PC1	3	91114590	1.64	2.37E-09	LCORL
PC6	35	1776352	0.31	8.26E-08	FOXQ1
	23	11346684	0.29	1.41E-07	TRAK1
Tibial Plateau Angle	10	28002796	2.01	2.25E-07	BET1, MYH9
	8	30830592	2.40	3.33E-07	WDHD1
Tibial Length	3	91114590	68.29	2.53E-08	LCORL
Diaphyseal Width Lateral Projection	3	91114590	0.59	6.13E-08	LCORL
Tuberosity Length	23	11389112	0.65	2.16E-07	TRAK1
Fat Pad Base	9	12074972	-0.28	4.47E-08	GH1
	3	91114590	0.22	1.60E-07	LCORL
Tibial Diaphyseal Width Cranial Caudal Projection	3	91114590	0.56	2.75E-09	LCORL
	9	12074972	-0.61	3.01E-07	GH1
Femoral Condyle Width Cranial Caudal Projection	3	91114590	1.65	7.58E-09	LCORL
Tibia Condyle Width Cranial Caudal Projection	3	91114590	3.88	4.53E-08	LCORL

https://doi.org/10.1371/journal.pone.0223094.t005

Table 6. Genome wide significant marker associations of 10 radiographic morphologic measurements and their principal components, chromosome position, effect size, p value and candidate genes in the associated interval following a multi-locus model GWAS performed using FarmCPU. Only significant locus associations have candidate genes listed. FarmCPU uses a 1% threshold for significance i.e. 0.01/number of markers used in GWAS = 6.9×10^{-8}. # indicates same locus as for the mixed linear model in GEMMA.

Phenotype	Chr	Position (bp)	Effect size	P-value	Candidate Genes
PC1	3	91114590	-0.96	3.11E-11#	LCORL
	X	29270503	0.67	5.93E-10	NPC2
	11	59866929	-0.94	7.65E-10	-
	9	43240534	0.77	1.07E-09	MYO18A
	6	74671230	-0.87	7.88E-09	NEGR1
	20	12792269	0.78	2.61E-08	ITPR1
PC4	16	30675811	-0.29	1.45E-14	-
	7	61531148	0.36	2.63E-14	CHST9
	13	50399261	-0.20	2.46E-10	-
	27	37583571	-0.13	2.57E-08	VMN2R
PC6	19	43088987	0.17	2.54E-14	SOCS2
	2	34373078	-0.26	1.89E-11	DIP2C
	29	38879394	-0.25	1.07E-10	PDP1
	24	16282763	-0.10	4.37E-08	GPCPD1
Tibial Length	3	91114590	-51.06	1.38E-17#	LCORL
	5	29898790	-58.56	4.04E-14	-
	11	59196021	48.73	5.14E-10	CYCL2
	24	43761051	40.55	1.69E-09	TUBB1
	6	26793945	21.95	3.65E-08	XYLT1
Tibial Diaphyseal Width Lateral Projection	14	23479385	0.29	5.14E-12	UMAD1
	3	91114590	-0.33	1.89E-10#	LCORL
	11	36466907	0.23	8.90E-10	BNC2
	30	13503286	0.24	7.09E-09	SEMA6D
Tuberosity Length	5	29898790	-0.39	2.32E-11	-
	23	11389112	-0.43	4.15E-10#	TRAK1
	3	91114590	-0.29	1.59E-08	LCORL
	33	29970487	0.27	2.28E-08	MELTF, DLG1
Fat Pad Base	3	91114590	-0.15	1.23E-12#	LCORL
	1	117449774	-0.10	3.45E-10	FXYD1, LGI4, HPN
	1	79362949	0.19	1.47E-08	TLE4
	37	672739	-0.20	2.23E-08	PMS1
Fat Pad Height	16	30712079	-0.01	1.36E-09	-
	37	25059163	0.01	4.93E-08	SLC11A, CATIP, CTDSP1

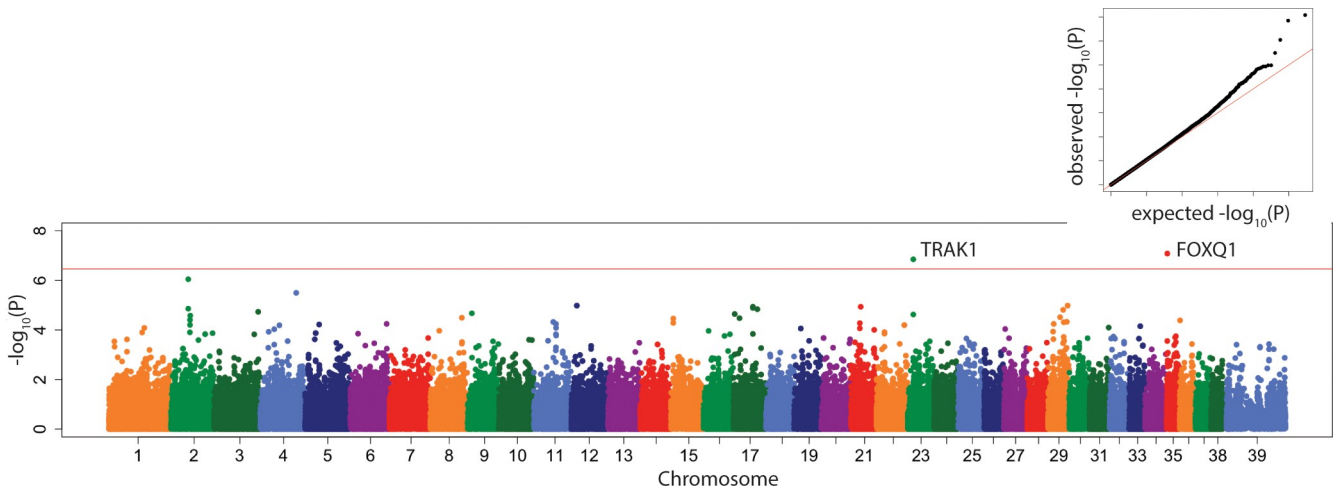https://doi.org/10.1371/journal.pone.0223094.t006

Fig 5. Manhattan plot of linear mixed model GWAS of PC6. Marker position plotted on the X axis against $-\log_{10}(P)$ on the Y axis. The Bonferroni adjusted genome wide p value threshold is drawn as the red line across the plot. QQ plot of expected $-\log_{10}(P)$ for no association against observed $-\log_{10}(P)$ is shown as insert.

stifle and hind limb that might be used as phenotypic screening tools to find breeding dogs with stifle conformation resistant to CCLD. Similarly, genetic markers and mutations, which are linked or causal for CCLD, will be relevant to improved breeding practices by eliminating dogs with strong genetic susceptibility from the breeding pool. Our goal here was to analyze radiographic measurements of stifle morphology by PCA and to perform a GWAS using published genotypes to find stifle morphologic features that might be under genetic control and thus amenable to practical breeding practices.

Six distinct radiographic dimensions and PC1 in both our GWAS models mapped to the same locus CFA03:91114590 which marks *LCORL*, a size-determining gene in several species. The effect sizes associated with this gene were large (Tables 5 and 6). Multiple measurements mapping to the same locus as PC1 supports the validity of the associations and suggests that *LCORL* is an important determinant of canine distal hind limb morphology. We reported
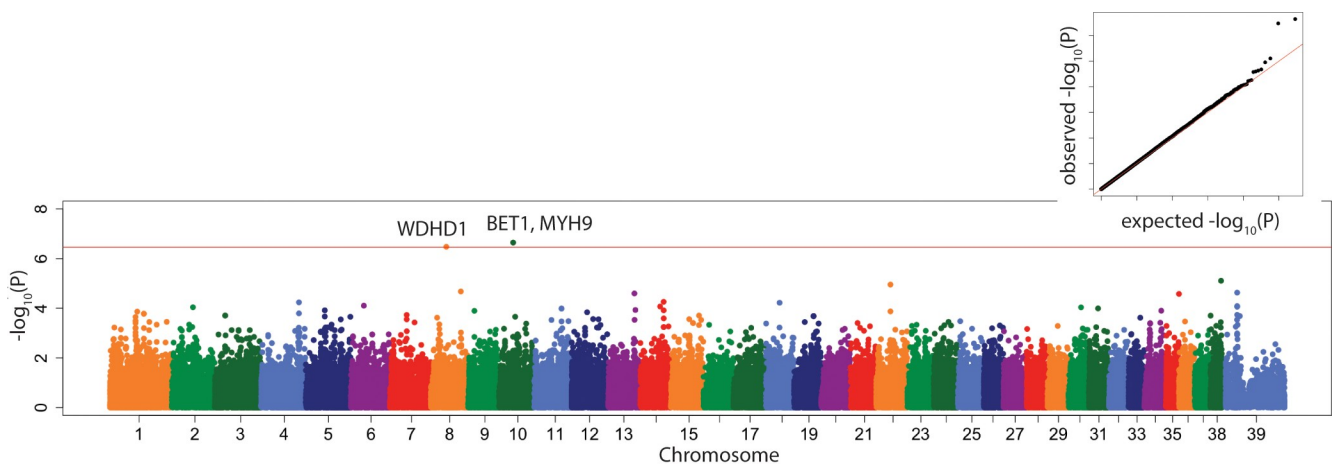

Fig 6. Manhattan plot of linear mixed model GWAS of tibial plateau angle. Marker position plotted on the X axis against $-\log_{10}(P)$ on the Y axis. The Bonferroni adjusted genome wide p value threshold is drawn as the red line across the plot. QQ plot of expected $-\log_{10}(P)$ for no association against observed $-\log_{10}(P)$ is shown as insert.

Fig 7. Manhattan plot of linear mixed model of cranial tibial diaphyseal length. Marker position plotted on the X axis against $-\log_{10}(P)$ on the Y axis. The Bonferroni adjusted genome wide p value threshold is drawn as the red line across the plot. QQ plot of expected $-\log_{10}(P)$ for no association against observed $-\log_{10}(P)$ is shown as insert.
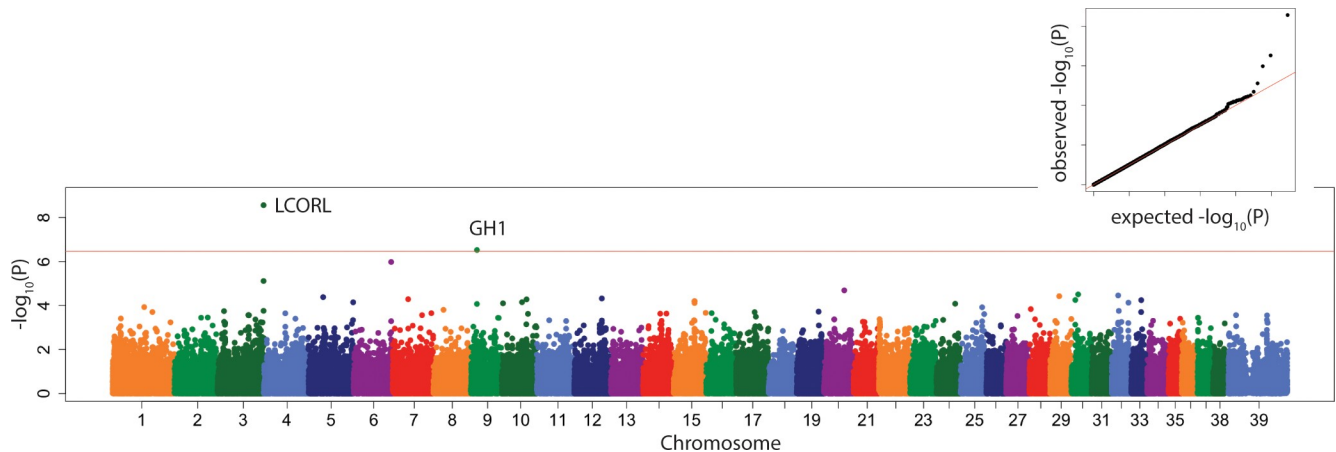
previously that PC1, as a composite average of pelvic radiographic dimensions, mapped to *IGF-1*, derived alleles of which are a major determinant of small body size in dogs.[19, 20, 27, 33] It is unclear why our GWAS of pelvic and stifle morphology showed significant association with two different growth factor-encoding genes, respectively. While IGF-1 is a potent growth factor for chondrocytes and therefore is important for normal growth plate activity, ligand-dependent nuclear receptor corepressor-like (*LCORL*) is a quantitative trait locus for body-size relevant traits in cattle, dogs, and horses. *LCORL* has been linked to arginine metabolism in growth[34] and can interact with C-terminal binding protein 1 (*CTBP1*), another transcriptional regulator.[35] A marker within another C-terminal binding protein (*CTBP2*) has been significantly associated with canine hip dysplasia using two mapping methods.[17,20] The locus CFA24:26793945 also had a large effect size (Table 6). The nearest candidate gene is *XYLT1*, a xylosyltransferase encoding gene, a key conserved regulator of chondrocyte differentiation and skeletal length.[36]

The CFAX:82 locus that was significantly associated with femoral and tibia condyle dimensions in the multi-locus GWAS model, has been fine mapped to the gene insulin receptor substrate 4 (*IRS4*), which also belongs to the IGF-1/growth hormone pathways[37] and acyl-CoA synthetase long-chain family member 4 (*ACSL4*), which has been associated with a muscly or stocky build in pigs and dogs[24, 29, 38, 39]. Other associated loci contain candidate genes which have been associated with skeletal growth and function (Table 6). Variants in *BNC2* (basonuclin 2), a highly conserved protein belonging to the C2H2 zinc finger proteins, have been associated with scoliosis is Japanese [40] and Chinese people.[41] A locus with the nearest candidate gene SEMA6D, an encoding member of the semaphorin family of cell surface or soluble proteins that regulate cell to cell interactions, was associated with tibial diaphyseal width and is expressed in osteoclasts.[42] *FRZB* (frizzled B related protein) is a major component of the WNT signaling pathway and is integral to chondrocyte development.[43]

Growth hormone 1 (*GH1*), the closest candidate gene at CFA09:12074972, which regulates body mass, was associated significantly with the length of the fat pad base and the width of the tibial diaphysis, in the linear mixed model only. The growth hormone-insulin-like growth factor-1 axis is critical to skeletal morphology and endosteal and periosteal osteoblastic activity must be synchronized to increase the width and mass of the diaphyseal cortex.[44–47] *GH1* has been associated with body size in humans and cattle.[33–35]

Fat pad compression, higher body weight, and younger age were all associated with CCLD in this study. Prior studies suggested that the association between body size and CCLD was more prominent within breeds, rather than across breeds,[2] whereas our study included many breeds. Dogs in this study with CCLD were younger than the control population in our study which is not consistent with other reports.[2] For our orthopedic genetic mapping studies, we selected control dogs over 8 years of age as available to allow potential genetic tendencies to be expressed [20], likely explaining the difference to previous reports. Both breed and sex can affect the age at which dogs succumb to CCLD.[48]

Dogs with CCLD had compressed infrapatellar fat pads, a well-recognized radiographic sign of synovitis, effusion, and stifle OA that results from CCLD.[49, 50] A recent study in human medicine found an association between a larger infrapatellar fat pad and decreased knee pain but reduced lateral tibial cartilage volume.[51] However, the infrapatellar fat pad exerts inflammatory effects in the stifle through its release of pro-inflammatory cytokines and alarmins like S100 facilitating the progression of OA. On the contrary, miR-100-5p-abundant exosomes derived from human infrapatellar fat pad mesenchymal stem cells protect articular cartilage via inhibition of mTOR in osteoarthritis which suggests a complex role for this fatty organ in knee/stifle degeneration. [52–54]

In the linear mixed model, PC6 (with a major negative weighting on fat pad base length) was significantly associated with locus CFA35:1,776,352 with the closest candidate gene *FOXQ1* (Fig 5). The volume of the infrapatellar fat pad, including its base length, as well as being related to the size of the dog, is also a function of the extent to which it is compressed by synovial effusion and synovitis that results from CCLD. The human FOXQ1 gene encodes a functional 403 amino acid protein, which has many physiological functions, including promoting epithelial differentiation, inhibiting smooth muscle differentiation, activating T cells and autoimmunity, and controlling mucin gene expression and granule content in stomach surface mucous cells. [55]

In our study, dogs with CCLD had significantly higher TPA, albeit a small elevation on average, compared to control dogs. Our average TPAs were lower than some studies but consistent with others.[56] While many studies have found associations between predictive factors for CCLD, including TPA and intercondylar notch width,[57] another study found that these factors, including TPA, do not predict bilateral rupture.[58] Fifty percent of a group of Labrador retrievers, after initial CCL rupture, tore the contralateral CCL within 5.5 months.[58] At present, clinicians have few useful tools besides body weight regulation, to advise owners about prevention of contralateral CCLD. It may be that a multivariate model which includes TPA might be predictive of CCLD but predicting CCLD risk in an individual dog is difficult with the tools veterinarians now have available.[59, 60] Axial and abaxial[61] TPAs and measures of tibial concavity and femoral condylar convexity might be more sensitive measurements of proclivity for CCLD[62] but require computed tomographic imaging. Lastly, other measures of stifle plateau mechanics, like the anatomic mechanical axis of the tibia, may be a more accurate predictor of CCLD.[12] In this study, even though the anatomic mechanical axis measurement was significantly correlated with the TPA (r = 0.74), the TPA had higher sensitivity and specificity (both above 0.9) and therefore was more accurate for predicting CCLD. One caveat in the referenced study was that CCLD-resistant breeds were compared to CCLD-susceptible breeds possibly exaggerating the potential advantage of this measurement.

Even though no heritability studies of TPA have been reported, the finding of a significant genetic marker association with TPA in the linear mixed model suggests that it may have a genetic basis and may be a path to improve stifle conformation and reduce CCLD risk in dogs. This finding would have to be replicated in order to encourage the application of TPA and/or genetic markers associated with TPA and CCLD in breeding programs to reduce its incidence. Tibial plateau angle was associated with a locus, using the linear mixed model, on CFA10:28,002,796 bp

with nearest candidate gene *BET1* (endoplasmic reticulum to Golgi function) and *TXN2* about 50kb upstream and *MYH9* about 80 kb downstream. MYH9-related disease is a rare autosomal-dominant disorder caused by mutations in this gene encoding non-muscle myosin heavy chain IIA. MYH9-related disease has a variable clinical evolution involving thrombocytopenia and possibly sensorineural deafness, cataract, and/or nephropathy often leading to end-stage renal disease. [63] Non-muscle myosin heavy chain IIA was shown to be integral to osteoclastogenesis and functions as a generator of cellular chemomechanical force.[64] Balanced osteoblast-osteoclast activity is important to normal growth plate function and its imbalance might affect TPA. A down-side to this significant association with TPA in our study which contained 77 Labrador retrievers is that we did not replicate the results of Baker *et al.*,[18] who associated a locus on CFA04 with TPA in 237 Labrador Retrievers only. Our study included multiple breeds. Interestingly, rupture of the anterior cruciate ligament in humans was recently associated with several morphological measurements on affected and control stifles including medial tibial posterior slope.[65]

As we have previously discussed[17], we did not obtain (or expect) identical results from application of both models. First of all, the genome wide threshold for the two models differed. The threshold for the FarmCPU method is more stringent at p<0.01 genome-wide. False positives in a GWAS can be effectively controlled by incorporation of genotype-based population structure and kinship among individuals to adjust the effect of a marker association. However, the adjustment for occult population structure can penalize the number of true positive associations. The FarmCPU approach extends previous mixed linear models into two separate stages. The fixed effect component tests each SNP, one at a time, with multiple associated markers (pseudo quantitative trait nucleotides) as covariates to control false positive associations. To avoid model over-fitting, the effect of the associated markers is then estimated as a random effect in the second stage by using them to define kinship. Previously, both real and simulated data analyses demonstrated that FarmCPU improved statistical power compared to current methods, while still controlling inflation [24].

Some limitations of this data included inconsistency of radiographic quality and a relatively small dataset for a PCA and for GWAS. The radiographs varied in positioning because they were used for two different osteotomy surgical planning procedures or for diagnosis of stifle disease, trauma and non-specific lameness. Although fixed traits within and across breeds can be mapped with hundreds of dogs, mapping complex, naturally segregating traits in dogs may require 500–1,000 cases and controls, and denser mapping arrays for adequate mapping power [20]. Because morphology and conformation underlie the fixed traits of breed height and body weight which conform to breed standards, the pure breed dogs in this study may have made identification of morphologic-based, locus associations possible with less that 500–1,000 dogs each group. Although more than two loci likely contribute to TPA, it seems important to replicate the associations of the genomic regions on chromosomes 3 and 10 with TPA in order to understand their effects on CCLD and to select against predisposing risk factors for CCLD.

Supporting information

S1 File. Table A. Excel file of 10 radiographic measurements performed in all 216 dogs with and without cranial cruciate ligament disease (CCLD). Figure A. Distributions of raw (left column) and transformed (right column) phenotypic data. a) tibia length b) lateral diaphysis c) tuberosity length d) fat pad base e) fat pad height f) cranial diaphysis g) femoral condyle h) femoral notch i) tibia condyle. Figure B. Manhattan plot of linear mixed model GWAS of transformed tibial length. Marker position plotted on the X axis against–log$_{10}$(P) on the Y axis. The Bonferroni adjusted genome wide p value threshold is drawn as the red line across the plot. QQ

plot of expected–$\log_{10}(P)$ for no association against observed–$\log_{10}(P)$ is shown as insert. Figure C. Manhattan plot of linear mixed model GWAS of transformed lateral tibial diaphyseal width. Marker position plotted on the X axis against–$\log_{10}(P)$ on the Y axis. The Bonferroni adjusted genome wide p value threshold is drawn as the red line across the plot. QQ plot of expected–$\log_{10}(P)$ for no association against observed–$\log_{10}(P)$ is shown as insert. Figure D. Manhattan plot linear mixed model GWAS of transformed tuberosity length. Marker position plotted on the X axis against–$\log_{10}(P)$ on the Y axis. The Bonferroni adjusted genome wide p value threshold is drawn as the red line across the plot. QQ plot of expected–$\log_{10}(P)$ for no association against observed–$\log_{10}(P)$ is shown as insert. Figure E. Manhattan plot of linear mixed model GWAS of transformed fat pad base. Marker position plotted on the X axis against–$\log_{10}(P)$ on the Y axis. The Bonferroni adjusted genome wide p value threshold is drawn as the red line across the plot. QQ plot of expected–$\log_{10}(P)$ for no association against observed–$\log_{10}(P)$ is shown as insert. Figure F. Manhattan plot of linear mixed model GWAS of transformed femoral condyle width. Marker position plotted on the X axis against–$\log_{10}(P)$ on the Y axis. The Bonferroni adjusted genome wide p value threshold is drawn as the red line across the plot. QQ plot of expected–$\log_{10}(P)$ for no association against observed–$\log_{10}(P)$ is shown as insert. Figure G. Manhattan plot of linear mixed model GWAS of transformed tibial condyle width. Marker position plotted on the X axis against–$\log_{10}(P)$ on the Y axis. The Bonferroni adjusted genome wide p value threshold is drawn as the red line across the plot. QQ plot of expected–$\log_{10}(P)$ for no association against observed–$\log_{10}(P)$ is shown as insert. Figure H. Manhattan plot of PC1 based on GWAS using FarmCPU modeling software. The Bonferroni adjusted genome wide p value threshold is drawn as the green line across the plot. QQ plot of observed versus expected distribution of p values for PC1 derived from the Farm CPU modeling software. Figure I. Manhattan plot of PC4 based on GWAS using FarmCPU modeling software. The Bonferroni adjusted genome wide p value threshold is drawn as the green line across the plot. QQ plot of observed versus expected distribution of p values for PC4 derived from the Farm CPU modeling software. Figure J. Manhattan plot of PC6 based on GWAS using Farm-CPU modeling software. The Bonferroni adjusted genome wide p value threshold is drawn as the green line across the plot. QQ plot of observed versus expected distribution of p values for PC6 derived from the Farm CPU modeling software. Figure K. Manhattan plot of transformed tibial length based on GWAS using FarmCPU modeling software. The Bonferroni adjusted genome wide p value threshold is drawn as the green line across the plot. QQ plot of observed versus expected distribution of p values for tibial length derived from the Farm CPU modeling software. Figure L. Manhattan plot of transformed tibial diaphyseal width based on GWAS using FarmCPU modeling software. The Bonferroni adjusted genome wide p value threshold is drawn as the green line across the plot. QQ plot of observed versus expected distribution of p values for transformed tibial diaphyseal width derived from the Farm CPU modeling software. Figure M. Manhattan plot of transformed tibial tuberosity length based on GWAS using Farm-CPU modeling software. The Bonferroni adjusted genome wide p value threshold is drawn as the green line across the plot. QQ plot of observed versus expected distribution of p values for transformed tibial tuberosity length derived from the Farm CPU modeling software. Figure N. Manhattan plot of transformed transformed infrapatellar fat pad height based on GWAS using FarmCPU modeling software. The Bonferroni adjusted genome wide p value threshold is drawn as the green line across the plot. QQ plot of observed versus expected distribution of p values for transformed infrapatellar fat pad height derived from the Farm CPU modeling software. Figure O. Manhattan plot of transformed transformed infrapatellar fat pad width based on GWAS using FarmCPU modeling software. The Bonferroni adjusted genome wide p value threshold is drawn as the green line across the plot. QQ plot of observed versus expected distribution of p values for transformed infrapatellar fat pad width derived from the Farm CPU

modeling software.Figure P. Manhattan plot of transformed transformed tibial diaphyseal width on the cranial caudal projection based on GWAS using FarmCPU modeling software. The Bonferroni adjusted genome wide p value threshold is drawn as the green line across the plot. QQ plot of observed versus expected distribution of p values for transformed tibial diaphyseal width on the cranial caudal view derived from the Farm CPU modeling software. Figure Q. Manhattan plot of transformed transformed femoral condyle width on the cranial caudal projection based on GWAS using FarmCPU modeling software. The Bonferroni adjusted genome wide p value threshold is drawn as the green line across the plot. QQ plot of observed versus expected distribution of p values for transformed femoral condyle width on the cranial caudal view derived from the Farm CPU modeling software. Figure R. Manhattan plot of transformed transformed tibial plateau width on the cranial caudal projection based on GWAS using FarmCPU modeling software. The Bonferroni adjusted genome wide p value threshold is drawn as the green line across the plot. QQ plot of observed versus expected distribution of p values for transformed tibial plateau width on the cranial caudal view derived from the Farm CPU modeling software. (DOCX)

Acknowledgments

Author Contributions

Conceptualization: Adam R. Boyko, Rory J. Todhunter.

Data curation: Eleni Healey, Jessica J. Hayward, Marta Castelhano, Adam R. Boyko, Rory J. Todhunter.

Formal analysis: Eleni Healey, Jessica J. Hayward, Adam R. Boyko, Rory J. Todhunter.

Funding acquisition: Rory J. Todhunter.

Investigation: Eleni Healey, Rachel J. Murphy, Jessica J. Hayward, Marta Castelhano, Adam R. Boyko, Rory J. Todhunter.

Methodology: Eleni Healey, Rachel J. Murphy, Jessica J. Hayward, Adam R. Boyko, Rory J. Todhunter.

Project administration: Rory J. Todhunter.

Resources: Marta Castelhano, Adam R. Boyko, Kei Hayashi, Ursula Krotscheck, Rory J. Todhunter.

Supervision: Jessica J. Hayward, Marta Castelhano, Adam R. Boyko, Rory J. Todhunter.

Writing – original draft: Eleni Healey, Rachel J. Murphy, Jessica J. Hayward, Rory J. Todhunter.

Writing – review & editing: Eleni Healey, Rachel J. Murphy, Jessica J. Hayward, Rory J. Todhunter.

References

1. Witsberger TH, Villamil A, Schultz LG, Hahn AW, Cook JL. Prevalence of and risk factors for hip dysplasia and cranial cruciate ligament deficiency in dogs. Journal of the American Veterinary Medical Association. 2008; 232:1818–24. https://doi.org/10.2460/javma.232.12.1818 PMID: 18598150

2. Taylor-Brown FE, Meeson RL, Brodbelt DC, Church DB, McGreevy PD, Thomson PC, et al. Epidemiology of cranial cruciate ligament disease diagnosis in dogs attending primary-care veterinary practices in England. Veterinary Surgery. 2015; 44:777–83. https://doi.org/10.1111/vsu.12349 PMID: 26118493

3. Whitehair JG, Vasseur PB, Willits NH. Epidemiology of cranial cruciate ligament rupture in dogs. Journal of the American Veterinary Medical Association. 1993; 203:1016–9. PMID: 8226247

4. An B, Xia J, Chang T, Wang X, Miao J, Xu L, et al. Genome-wide association study identifies loci and candidate genes for internal organ weights in Simmental beef cattle. Physiologic Genomcis. 2018; 50 (7):523–31.

5. Adams P, Bolus R, Middleton S, Moores AP, Grierson J. Influence of signalment on developing cranial cruciate rupture in dogs in the UK. Journal of Small Animal Practice. 2011; 52:347–52. https://doi.org/10.1111/j.1748-5827.2011.01073.x PMID: 21651558

6. Duval JM, Budsberg SC, Flo GL, Sammarco JL. Breed, sex, and body weight as risk factors for rupture of the cranial cruciate ligament in young dogs. Journal of the American Veterinary Medical Association. 1999; 215:811–4. PMID: 10496133

7. Ekenstedt KJ, Minor KM, Rendahl AK, Conzemius MG. *DNM1* mutation status, sex, and sterilization status of a cohort of Labrador retrievers with and without cranial cruciate ligament rupture. Canine Genetics and Epidemiology. 2017; 4:2. https://doi.org/10.1186/s40575-017-0041-9 PMID: 28168039

8. Morris E, Lipowitz AJ. Comparison of tibial plateau angles in dogs with and without cranial cruciate ligament injuries. Journal of the American Veterinary Medical Association. 2001; 218:363–6. https://doi.org/10.2460/javma.2001.218.363 PMID: 11201561

9. Haynes KH, Biskup A, Freeman A, Conzemius MG. Effect of tibial plateau angle on cranial cruciate ligament strain: an ex vivo study in the dog. Veterinary Surgery. 2015; 44:46–9. https://doi.org/10.1111/j.1532-950X.2014.12219.x PMID: 24902869

10. Reif U, Probst CW. Comparison of tibial plateau angles in normal and cranial cruciate deficient stifles of Labrador retrievers. Veterinary Surgery. 2003; 32:385–9. https://doi.org/10.1053/jvet.2003.50047 PMID: 12866002

11. Fujita Y, Hara Y, Ochi H, Nezu Y, Harada Y, Yogo T, et al. 'The possible role of the tibial plateau angle for the severity of osteoarthritis in dogs with cranial cruciate ligament rupture. Journal of Veterinary Medical Science. 2006; 68(7):675–9. https://doi.org/10.1292/jvms.68.675 PMID: 16891779

12. Guénégo L, Payot M, Charru P, Verwaerde P. Comparison of tibial anatomical-mechanical axis angle between predisposed dogs and dogs at low risk for cranial cruciate ligament rupture. Veterinary Journal. 2017; 225:35–41.

13. Wilke VL, Zhang S, Evans RB, Conzemius MG, Rothschild MF. Identification of chromosomal regions associated with cranial cruciate ligament rupture in a population of Newfoundlands. American Journal of Veterinary Research. 2009; 70(8):1013–7. https://doi.org/10.2460/ajvr.70.8.1013 PMID: 19645583

14. Baird AEG, Carter SD, Innes JF, Ollier WE, Short AD. Genome-wide association study identifies genomic regions of association for cruciate ligament rupture in Newfoundland dogs. Animal Genetics. 2014b; 45:542–9. https://doi.org/10.1111/age.12162 PMID: 24835129

15. Baird AEG, Carter SD, Innes JF, Ollier WE, Short AD. Genetic basis of cranial cruciate ligament rupture (CCLR) in dogs. Connective Tissue Research. 2014a; 55:275–81. https://doi.org/10.3109/03008207.2014.910199 PMID: 24684544

16. Baker LA, Kirkpatrick B, Rosa GJ, Gianola D, Valente B, Sumner JP, et al. Genome-wide association analysis in dogs implicates 99 loci as risk variants for anterior cruciate ligament rupture. PLos One. 2017; 12:e0173810. https://doi.org/10.1371/journal.pone.0173810 PMID: 28379989

17. Huang M, Hayward JJ, Corey E, Garrison SJ, Wagner GR, Krotscheck U, et al. A novel iterative mixed model to remap three complex orthopedic traits in dogs. PLoS One. 2017; 12:e0176932. https://doi.org/10.1371/journal.pone.0176932 PMID: 28614352

18. Baker LA, M. RGJ, Hao Z, Piazza A, Hoffman C, Binversie EE, et al. Multivariate genome-wide association analysis identifies novel and relevant variants associated with anterior cruciae ligament rupture risk in the dog model. BMC Genetics. 2018; 19(1):39. https://doi.org/10.1186/s12863-018-0626-7 PMID: 29940858

19. Fealey MJ, Li J, Todhunter RJE, Krostscheck U, Hayashi K, McConkey MJ, et al. Genetic mapping of principal components of canine pelvic morphology. Canine Genetics and Epidemiology. 2017; 4:4. https://doi.org/10.1186/s40575-017-0043-7 PMID: 28352471

20. Hayward JJ, Castelhano MG, Oliveira KC, Corey E, Balkman C, Baxter TL, et al. Complex disease and phenotype mapping in the domestic dog. Nature Communications. 2016; 7:10460. https://doi.org/10.1038/ncomms10460 PMID: 26795439

21. Team RC. A language and environment for statistical computing: https://www.R-project.org/; 2018.

22. Purcell S, Neale B, Todd-Brown K, Ferreira MA, Bender D, Maller J, et al. PLINK: a tool set for whole-genome association and population-based linkage analyses. American Journal of Human Genetics. 2007; 81:559–75. https://doi.org/10.1086/519795 PMID: 17701901

23. Zhou X, Stephens M. Genome-wide efficient mixed-model analysis for associatoin studies. Naure Genetics. 2012; 44:821–4.

24. Liu X, Huang M, Fan B, Buckler ES, Zhang Z. Iterative Usage of Fixed and Random Effect Models for Powerful and Efficient Genome-Wide Association Studies. PLoS Genet. 2016; 12(2):e1005767. https://doi.org/10.1371/journal.pgen.1005767 PMID: 26828793; PubMed Central PMCID: PMC4734661.

25. Brooks SA, Stick J, Braman A, Palermo K, Robinson NE, Ainsworth DM. Identification of loci affecting sexually dimorphic patterns for height and recurrent laryngeal neuropthy risk in American Belgian draft horses. Physiologic Genomcis. 2018;(September 28).

26. Bhuiyan MSA, Lim D, Park M, Lee S, Kim Y, Gondro C, et al. Functional partitioning of genomic variance and genome-wide association study for carcass traits in Korean Hanwood cattle using imputed sequence level SNP data. Frontiers in Genetics. 2018; 9:217. https://doi.org/10.3389/fgene.2018.00217 PMID: 29988410

27. Boyko AR, Quignon P, Li L, Schoenebeck JJ, Degenhardt JD, Lohmueller KE, et al. A simple genetic architecture underlies morphological variation in dogs. PLoS biology. 2010; 8(8):e1000451. https://doi.org/10.1371/journal.pbio.1000451 PMID: 20711490

28. Vaysse A, Ratnakumar A, Derrien T, Axelsson E, Rosengren Pielberg G, Sigurdsson S, et al. Identification of genomic regions associated with phenotypic variation between dog breeds using selection mapping. PLoS genetics. 2011; 7(10):e1002316. https://doi.org/10.1371/journal.pgen.1002316 PMID: 22022279

29. Plassais J, Rimbault M, Williams FJ, Davis BW, Schoenebeck JJ, Osrander EA. Analysis of large versus small dogs reveals three genes on the canine X chromosome associated with body weight, muscling and back fat thickness. PLoS Genet. 2017; 13(3):e1006661. https://doi.org/10.1371/journal.pgen.1006661 PMID: 28257443

30. Wilke VL, Robinson DA, Evans RB, Rothschild MF, Conzemius MG. Estimate of the annual economic impact of treatment of cranial cruciate ligament injury in dogs in the United States. Journal of the American Veterinary Medical Association. 2005; 227(10):1604–7. https://doi.org/10.2460/javma.2005.227.1604 PMID: 16313037

31. von Pfeil DJF, Kowaleski MP, Glassman M, Dejardin LM. Results of a survey of Veterinary Orthopedic Society members on the preferred method for treating cranial cruciate ligament rupture in dogs weighing more than 15 kilogams (33 pounds). Journal of the American Veterinary Medical Association. 2018; 253 (5):586–5997. https://doi.org/10.2460/javma.253.5.586 PMID: 30110219

32. Wilke VL, Conzemius MG, Kinghorn BP, Macrossan PE, Cai W, Rothschild MF. Inheritance of rupture of the cranial cruciate ligament in Newfoundlands. Journal of the American Veterinary Medical Association. 2006; 228(1):61–4. https://doi.org/10.2460/javma.228.1.61 PMID: 16426167

33. Sutter NB, Bustamante CD, Chase K, Gray MM, Zhao K, Zhu L, et al. A single IGF1 allele is a major determinant of small size in dogs. Science. 2007; 316:112–5. https://doi.org/10.1126/science.1137045 PMID: 17412960

34. Weikard R, Altmaier E, Suhre K, Weinberger KM, Hammon HM, Albrecht E, et al. Metabolomic profiles indicate distinct physiological pathways affected by two loci with major divergent effect on Bos taurus growth and lipid deposition. Physiologic Genomcis. 2010; 42A(2):79–88.

35. Vinayagam A, Stelzl U, Foulle R, Plassmann S, Zenkner M, Timm J, et al. A directed protein interaction network for investigating intracellular signal transduction. Science Signaling. 2011; 4(189):rs8. https://doi.org/10.1126/scisignal.2001699 PMID: 21900206

36. Mis EK, Liem KFJ, Kong Y, Schwartz NB, Domowicz M, Weatherbee SD. Forward genetics defines Xylt1 as a key, conserved regulator of early chondrocyte maturation and skeletal length. Developmental Biology. 2014; 385(1):67–82. https://doi.org/10.1016/j.ydbio.2013.10.014 PMID: 24161523

37. Qu BH, Karas M, Koval A, LeRoth D. Insulin receptor substrate-4 enhances insulin-like growth factor-l-induced cell proliferation. Journal of Biological Chemistry. 1999; 274:31179–84. https://doi.org/10.1074/jbc.274.44.31179 PMID: 10531310

38. Ma J, Gilbert H, Iannuccelli N, Duan Y, Guo B, Huang W, et al. Fine mapping of fatness QTL on porcine chromosome X and analyses of three positional candidate genes. BMC Genetics. 2013; 14:46. https://doi.org/10.1186/1471-2156-14-46 PMID: 23725562

39. Cepica S, Batenschlager H, Geldermann H. Mapping of QTL on chromosome X for fat deposition, muscling and growth traits in a wild boar x Meishan F2 family using a high-densityi gene map. Animal Genetics. 2007; 38:634–8. https://doi.org/10.1111/j.1365-2052.2007.01661.x PMID: 17931399

40. Ikegawa S. Genomic study of adolescent idiopathic scoliosis in Japan. Scoliosis Spinal Disorders. 2016; 11:5. https://doi.org/10.1186/s13013-016-0067-x PMID: 27299157

41. Xu L, Xia C, Quin X, Sun W, Tang NL, Qiu Y, et al. Genetic variant of BNC2 gene is functionally associated with adolescent idiopathic scoliosis in Chinese population. Molecular Genetics and Genomics. 2017; 292(4):789–95. https://doi.org/10.1007/s00438-017-1315-3 PMID: 28342042

42. Deng X, Liang LN, Zhu D, Zheng LP, Yu JH, Meng XL, et al. Wedelolactone inhibitics osteoclastogenesis but enhances osteoblastogenesis through altering different semaphorins production. International Immunopharmacology. 2018; 60:41–9. https://doi.org/10.1016/j.intimp.2018.04.037 PMID: 29702282

43. Zhong L, Huang X, Rodrigues ED, Leijten JC, Verrips T, El Khattabi M, et al. Endogenous DDK1 and FRZB regulate chondrogenesis and hypertrophy in three-dimensional cultures of human chondrocytes and human mesenchymal stem cells. Stem Cells and Development. 2016; 25(23):1808–17. https://doi.org/10.1089/scd.2016.0222 PMID: 27733096

44. Liu Z, Mohan S, Yakar S. Does the GH/GF-1 axis contribute to skeletal sexual dimorphism? Evidence from mouse studies. Growth Hormone IGF Research. 2016; 27:7–17. https://doi.org/10.1016/j.ghir.2015.12.004 PMID: 26843472

45. Millar DS, Lewis MD, Horan M, Newsway V, Easter TE, Gregory JW, et al. Novel mutations of the growth hormone 1 (GH1) gene disclosed by modulation of the clinical selection criteria for individuals with short stature. Human Mutation. 2003; 21(4):424–240. https://doi.org/10.1002/humu.10168 PMID: 12655557

46. Mullen MP, Berry DP, Howard DJ, Diskin MG, Lynch CO, Berkowicz EW, et al. Associations between novel single nucleotide polymorphisms in the Bos taurus growth hormone gene and performance traits in Holstein-Friesian dairy cattle. Journal of Dairy Science. 2010; 93(12):5959–69. https://doi.org/10.3168/jds.2010-3385 PMID: 21094770

47. Lango Allen H, Lango Allen H, Estrada K, Lettre G, Berndt SI, Weedon MN, et al. Hundreds of variants clustered in genomic loci and biological pathways affect human height. Nature. 2010; 467(7317):832–8. https://doi.org/10.1038/nature09410 PMID: 20881960

48. Guthrie JW, Keeley BJ, Maddock E, Bright SR, May C. Effect of signalment on the presentation of canine patients suffering from cranial cruciate ligament disease. Journal of Small Animal Practice. 2012; 53(5):273–37. https://doi.org/10.1111/j.1748-5827.2011.01202.x PMID: 22489873

49. Widmer WR, Buckwalter KA, Braunstein EM, Hill MA, O'Connor BL, Visco DM. Radiographic and magnetic resonance imaging of the stifle joint in experimental osteoarthritis of dogs. Veterinary Radiology and Ultrasound. 1994; 35(5):371–84.

50. Fuller MC, Mayashi K, Bruecker KA, Holsworth IG, Sutton JS, Kass PH, et al. Evaluation of the radiographic infrapatellar fat pad sign of the contralateral stifle joint as a risk factor for subsequent contralateral cranial cruciate ligament rupture in dogs with unilateral rupture: 96 cases (2006–2007). Journal of the American Veterinary Medical Association. 2014; 244(3):328–38. https://doi.org/10.2460/javma.244.3.328 PMID: 24432965

51. Teichtahl AJ, Wulidasari E, Brady SR, Wang Y, Wluka AE, Ding C, et al. A large infrapatellar fat pad protects against knee pain and lateral tibial cartilage volume loss. Arthritis Research and Therapy. 2015; 17:318. https://doi.org/10.1186/s13075-015-0831-y PMID: 26555322

52. Schmidli MR, Fuhrer B, Kurt N, Senn D, Drögemüller M, Rytz U, et al. Inflammatory pattern of the infrapatellar fat pad in dogs with canine cruciate ligament disease. BMC Veterinary Research. 2018; 14:161. https://doi.org/10.1186/s12917-018-1488-y PMID: 29769086

53. Wu J, Kuang L, Chen C, Yang J, Zeng WN, Li T, et al. miR-100-5p-abundant exosomes derived from infrapatellar fat pad MSCs protect articular cartilage and ameliorate gait abnormalities via inhibition of mTOR in osteoarthritis. Biomaterials. 2019; 206:87–100. https://doi.org/10.1016/j.biomaterials.2019.03.022 PMID: 30927715

54. Belluzzi E, Stocco E, Pozzuoli A, Granzotto M, Porzionato A, Vettor R, et al. Contribution of infrapatellar fat pad and synovial membrane to knee osteoarthritis pain. BioMed Research International. 2019; (March 31):Article ID 6390182.

55. Yang L, Zhang Y, Zhendong Y, Li S, Zhenhua Y, Xu M. Forkhead box Q1: a key player in the pathogenesis of tumors (review). International Journal of Oncology. 2016; 49(1):51–8. https://doi.org/10.3892/ijo.2016.3517 PMID: 27176124

56. Glassman M, Hofmeiser E, Weh JM, Roach W, Torres B, Johnston S, et al. Radiographic quantitative assessment of caudal proximal tibial angulation in 100 dogs with cranial cruciate ligament rupture. Veterinary Surgery. 2011; 40(7):830–8. https://doi.org/10.1111/j.1532-950X.2011.00857.x PMID: 21906096

57. Kyllar M, Čížek P. Cranial cruciate ligament structure in relation to the tibial plateau slope and intercondylar notch width in dogs. Journal of Veterinary Science. 2018; 19(5):699–707. https://doi.org/10.4142/jvs.2018.19.5.699 PMID: 29929359

58. Buote N, Fusco J, Radasch R. Age, tibial plateau angle, sex, and weight as risk factors for contralateral rupture of the cranial cruciate ligament in Labradors. Veterinary Surgery. 2009; 38:481–9. https://doi.org/10.1111/j.1532-950X.2009.00532.x PMID: 19538670

59. Cunningham DP, Mostafa AA, Gordan-Evans WJ, Boudrieau RJ, Griffon DJ. Factors contributing to the variability of a predictive score for cranial cruciate ligament deficiency in Labrador retrievers. BMC Veterinary Research. 2017; 13(1):235. https://doi.org/10.1186/s12917-017-1154-9 PMID: 28806971

60. Janovec J, Kyllar M, Midgley D, Owen M. Conformation of the proximal tibia and cranial cruciate ligament disease in small breed dogs. Veterinary and Comparative Orthopaedics and Traumatology. 2017; 30(3):178–83. https://doi.org/10.3415/VCOT-16-07-0115 PMID: 28331933

61. Wilke VL, Conzemius MG, Besancon MF, Evans RB, Ritter M. Comparison of tibial plateau angle between clinically normal greyhounds and Labrador retrievers with and without rupture of the cranial cruciate ligament. Journal of the American Veterinary Medical Association. 2002; 221(10):1426–9. https://doi.org/10.2460/javma.2002.221.1426 PMID: 12458611

62. Townsend S, Kim SE, Tinga S. Tibial plateau morphology in dogs with cranial cruciate ligament insufficiency. Veterinary Surgery. 2018; 47(8):1009–15. https://doi.org/10.1111/vsu.12953 PMID: 30303540

63. Pecci A, Klersy C, Gresele P, De Rocco D, Bozzi V, Russo G, et al. MYH9-related disease: a novel prognostic model to predict the clinical evolution of the disease based on genotype-phenotype correlations. Human Mutation. 2014; 35(2):236–47. https://doi.org/10.1002/humu.22476 PMID: 24186861

64. McMichael BK, Wysolmerski RB, Lee BS. Regulated proteolysis of nonmuscle myosin IIA stimulates osteoclast fusion. Journal of Biological Chemistry. 2009; 284(18):12266–75. https://doi.org/10.1074/jbc.M808621200 PMID: 19269977

65. Kızılgöz V, Sivrioğlu AK, Ulusoy GR, Aydın H, Karayol SS, Menderes U: Analysis of the risk factors for anterior cruciate ligament injury: an investigation of structural tendencies. Clin Imaging. 2018; 50:20–30. https://doi.org/10.1016/j.clinimag.2017.12.004 PMID: 29253746